International Journal of Imaging Systems and Technology

WILEY

RESEARCH ARTICLE OPEN ACCESS

Machine Learning–Based Cardiovascular Risk Classification Using Dynamic Time-Series Features From Carotid Duplex Sonography

Belilla Yonas Befirdu[1] | Duc-Manh Dinh[1] | Eui-Young Choi[2] | Kyehan Rhee[1]

[1]Department of Mechanical Engineering, Myongji University, Yongin-si, Gyeonggi-do, Republic of Korea | [2]Division of Cardiology, Gangnam Severance Hospital, Yonsei University College of Medicine, Seoul, Republic of Korea

Correspondence: Kyehan Rhee (khanrhee@mju.ac.kr)

Received: 11 March 2026 | **Revised:** 20 April 2026 | **Accepted:** 25 April 2026

Keywords: arterial dynamics | carotid duplex sonography | feature selection | machine learning | plaque burden | time series data analysis

ABSTRACT

Although carotid duplex sonography provides comprehensive hemodynamic and morphological information, clinical assessments typically rely on limited static features and flow velocity measurements. This study investigated the feasibility of applying machine learning to classify cardiovascular disease (CVD) risk using dynamic arterial time-series data derived from carotid diameter, flow velocity, and brachial pulse pressure waveforms. Signal-derived and shapelet-based features were extracted and selected using the minimum redundancy maximum relevance algorithm, and eight classifiers were evaluated. Integrating signal-derived and shapelet-based features improved classification accuracy to 0.90, compared with 0.77 and 0.80 for each feature set alone. Among the models, the random forest classifier achieved the best performance (accuracy 0.90, AUC 0.95, F1-score 0.80). The combined use of diameter, velocity, and pressure waveforms yielded the highest accuracy, demonstrating that dynamic carotid time-series data provide complementary information for CVD risk classification. These findings highlight the potential of machine learning–based ultrasound time-series analysis as a complementary, data-driven approach to conventional static imaging for CVD assessment.

1 | Introduction

Atherosclerosis is a chronic, progressive vascular disease marked by the buildup of lipid-rich plaques within arterial walls. This accumulation narrows the vessel lumen, impedes blood flow, and significantly increases the risk of cardiovascular diseases (CVD), including stroke and myocardial infarction [1, 2]. Carotid duplex sonography is a non-invasive imaging technique that combines B-mode and Doppler ultrasound to provide real-time assessment of both structural and hemodynamic characteristics of the carotid arteries. Owing to its safety, cost-effectiveness, portability, and absence of radiation exposure, it is widely utilized in clinical settings. This modality has been employed to identify and characterize atherosclerotic plaques, as well as estimating the severity of arterial stenosis [3]. B-mode ultrasound provides morphological information on arterial walls, and parameters such as intima-media thickness (IMT), total plaque area (TPA), maximum plaque height, and plaque texture (echogenicity) have been recognized as important clinical risk factors [4].

Increased IMT has been consistently associated with elevated risk of myocardial infarction and stroke, as demonstrated in large population-based studies such as the Atherosclerosis Risk in Communities study [5] and the Rotterdam Study [6], reflecting cumulative atherosclerotic burden. Similarly, TPA has been shown to be a stronger predictor of future cardiovascular events than IMT alone [7]. Plaque composition and echogenicity are also linked to plaque vulnerability, with echolucent plaques being associated with higher risk of rupture

and embolic events [8]. Spectral Doppler sonography is used primarily to quantify velocity elevations at sites of stenosis [9]. Quantitative blood flow parameters, including peak systolic velocity (PSV), end-diastolic velocity (EDV), and mean velocity, provide not only estimates of stenosis severity but also indirect measures of downstream vascular resistance and arterial compliance [10]. Derived indices such as the resistive index (RI) and pulsatility index (PI) reflect microvascular resistance and arterial stiffness, and have been associated with increased cardiovascular morbidity and mortality [11, 12]. Despite the comprehensive information offered by carotid duplex sonography, clinical assessments typically focus on a limited set of features primarily plaque thickness, morphology and flow velocity. Increasing attention has been given to arterial wall kinematics—such as radial and longitudinal motion, velocity, and strain within plaque regions—as potential markers for improved risk stratification.

These biomechanical parameters are closely related to arterial stiffness and plaque stability, with reduced strain and abnormal motion patterns being associated with higher cardiovascular risk [13]. Arterial dynamics, including pressure, wall distension, and flow velocity waveforms, also provide valuable information on vascular aging [14] and disease progression. For example, reduced arterial distensibility and altered waveform morphology are indicative of increased vascular stiffness and impaired hemodynamic regulation [15]. Relationships among these waveforms, expressed through correlations or ratios, reflect arterial viscoelasticity [16] and vascular impedance [17], both of which have been linked to cardiovascular risk and target organ damage. Despite these advances, relatively few studies have leveraged dynamic ultrasound imaging [18] or spectral Doppler waveform data [19] for comprehensive CVD risk prediction.

In recent years, artificial intelligence has emerged as a powerful tool in ultrasound imaging, capable of extracting, analyzing, and interpreting complex quantitative features. AI-based approaches have been developed to characterize plaque morphology and texture, thereby aiding CVD risk prediction and classification [20, 21]. Beyond imaging-based analysis, machine learning (ML) has demonstrated broad utility across cardiology, including the estimation of central hemodynamics from peripheral signals via learned transfer functions, enabling non-invasive reconstruction of central blood pressure and flow characteristics [22]. ML techniques have also been applied to the prediction and quantification of arterial stiffness—an important biomarker of vascular aging and cardiovascular risk—using multimodal physiological data [23], as well as to large-scale cardiovascular event prediction through integration of clinical and physiological variables [24].

Despite these advances, most existing ultrasound-based studies have focused on static plaque imaging, with limited attention given to arterial dynamics [25]. Dynamic arterial features, such as wall motion and Doppler flow velocity, remain underexplored, despite their strong physiological relevance to vascular function and cardiovascular risk. This study investigates the feasibility of applying machine learning to classify CVD risk using dynamic arterial time-series data, specifically radial wall motion and spectral Doppler velocity waveforms acquired via carotid duplex sonography.

2 | Method

2.1 | Study Population

Participants were retrospectively selected from patients who underwent both carotid duplex ultrasound (US) and brachial-to-ankle pulse wave velocity (PWV) measurements on the same day at Gangnam Severance Hospital, Seoul, Korea. The inclusion criteria comprised individuals aged ≥ 50 years who were referred for cardiovascular risk evaluation in a clinical setting. Exclusion criteria included: (1) poor ultrasound image quality precluding reliable arterial wall boundary delineation; (2) incomplete or excessively noisy waveform signals; and (3) comorbid conditions known to significantly affect arterial hemodynamics (e.g., severe arrhythmia or advanced heart failure). A total of 150 individuals (117 males and 33 females; mean age 66.8 ± 6.2 years) were included in the final analysis. All imaging data were stored in digital format and analyzed offline under standardized processing conditions. The study protocol was approved by the Institutional Review Board of Gangnam Severance Hospital (IRB No. 3-2020-01420).

2.2 | Data Acquisition

For each participant, either the right or left common carotid artery was selected for analysis. Longitudinal B-mode cine images were acquired 2–3 cm proximal to the carotid bifurcation, capturing at least two full cardiac cycles. Images were recorded at 25 frames per second with a spatial resolution of 50–70 μm/pixel. In the first frame of each sequence, the lumen–intima interfaces of both near and far walls were manually annotated. Arterial wall motion was then automatically tracked using CAROLAB (CREATIS, Lyon, France), which applies a speckle-tracking algorithm based on block matching guided by the segmented contours [26]. The lumen diameter was measured ten times per frame and averaged to generate the diameter waveform. The maximum standard deviation across repeated measurements was less than 5% of the measured diameter, indicating good reproducibility. Carotid flow velocity waveforms were obtained from spectral Doppler images at the same anatomical location as the diameter measurements. A single cardiac cycle, defined from R-wave to R-wave of the electrocardiogram (ECG), was extracted. The velocity envelope was derived using gray-level threshold-based binarization, isolating the maximal Doppler spectrum based on peak systolic intensity. The upper boundary of the binarized spectrum was then used as the velocity time series and low-pass filtered at 10 Hz. Brachial pressure waveforms were recorded using a volume plethysmography system (VP-1000 Plus, Omron, Japan). As the device does not provide an explicitly defined digital sampling rate, the exported waveforms were resampled to 128 Hz for subsequent analysis to ensure consistency with other synchronized signals [27].

2.3 | Data Processing and Signal Preparation

Diameter waveforms were detrended, low-pass filtered at 8 Hz to remove motion artifacts and high-frequency noise, and resampled at 128 Hz. Diameter, velocity, and pressure signals

were synchronized using ECG, aligned to the R-wave peak, and normalized to one cardiac cycle. Specifically, cardiac cycles were identified using the R-wave peak of the ECG signal as a fiducial marker. The diameter and velocity waveforms were temporally aligned based on this reference to ensure consistent phase correspondence across signals. Each signal was then segmented into individual cardiac cycles, and a representative cycle was selected and time-normalized to a fixed length (i.e., rescaled in time) to reduce inter-beat variability while preserving key physiological features. The resulting synchronized signals were used as multivariate time-series inputs for subsequent analysis.

2.4 | Risk Stratification

Participants were classified into high- and low-risk groups based on total plaque area (TPA), as illustrated in Figure 1. TPA was calculated as the sum of plaque areas within the carotid segments where diameter measurements were obtained, as assessed by experienced clinicians. TPA has been shown to correlate strongly with coronary heart disease [28] and to improve CVD risk prediction [29, 30]. A threshold of 40 mm^2 was used to define high-risk status. This cutoff was based on prior evidence from Korean patients with suspected coronary artery disease [31] and is consistent with ranges associated with elevated cardiovascular risk in comparable populations [28]. Among the 150 participants, 113 were classified as low risk and 37 as high risk.

2.5 | Feature Extraction and Selection

Conventional ML classifiers were employed for CVD risk prediction due to their simplicity, interpretability, and suitability for relatively small datasets, in contrast to neural networks, which typically require larger datasets and are less interpretable. In the ML pipeline, feature extraction constituted a critical initial step. Features were extracted from the three ECG-synchronized waveforms using the Time Series Feature Extraction Library (TSFEL) and the Shapelet Transform. TSFEL facilitated automated extraction of signal-derived features including statistical (e.g., mean, variance, skewness), temporal (e.g., zero-crossing rate, autocorrelation), and spectral (e.g., dominant frequency, spectral entropy) descriptors [32]. To reduce dimensionality and prevent overfitting, the Maximum Relevance Minimum Redundancy (mRMR) algorithm was applied [33], selecting features that maximized relevance (F-value) while minimizing redundancy (mean Pearson correlation). Feature selection was performed exclusively on the training data following the stratified train–test split. The selected feature subset was then fixed and applied to the held-out test set for performance evaluation. Additionally, shapelet analysis was used to extract short, discriminative subsequences from the multivariate time series. Shapelets were derived across all three waveforms, and each time series was represented by a feature vector of Euclidean distances to these three-dimensional shapelets, which were z-normalized to avoid high-magnitude dominance [34]. To reduce computational cost during mutual information (MI) calculation and subsequent scoring, histogram binning was applied, while the original distances were retained for modeling [35]. TSFEL and shapelet features were then fused to form a combined set capturing complementary signal-derived and subsequence information.

2.6 | Machine Learning Models

Eight ML algorithms spanning different methodological families were employed to classify CVD risk, capturing both

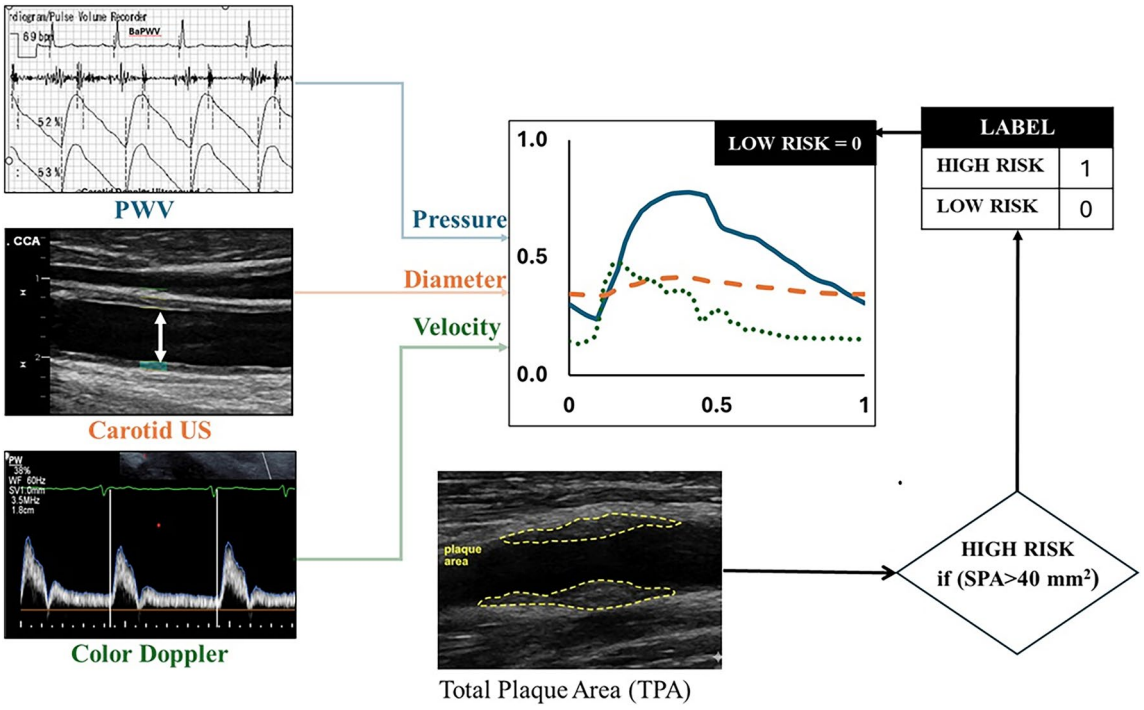

FIGURE 1 | Overview of the data acquisition and labeling process.

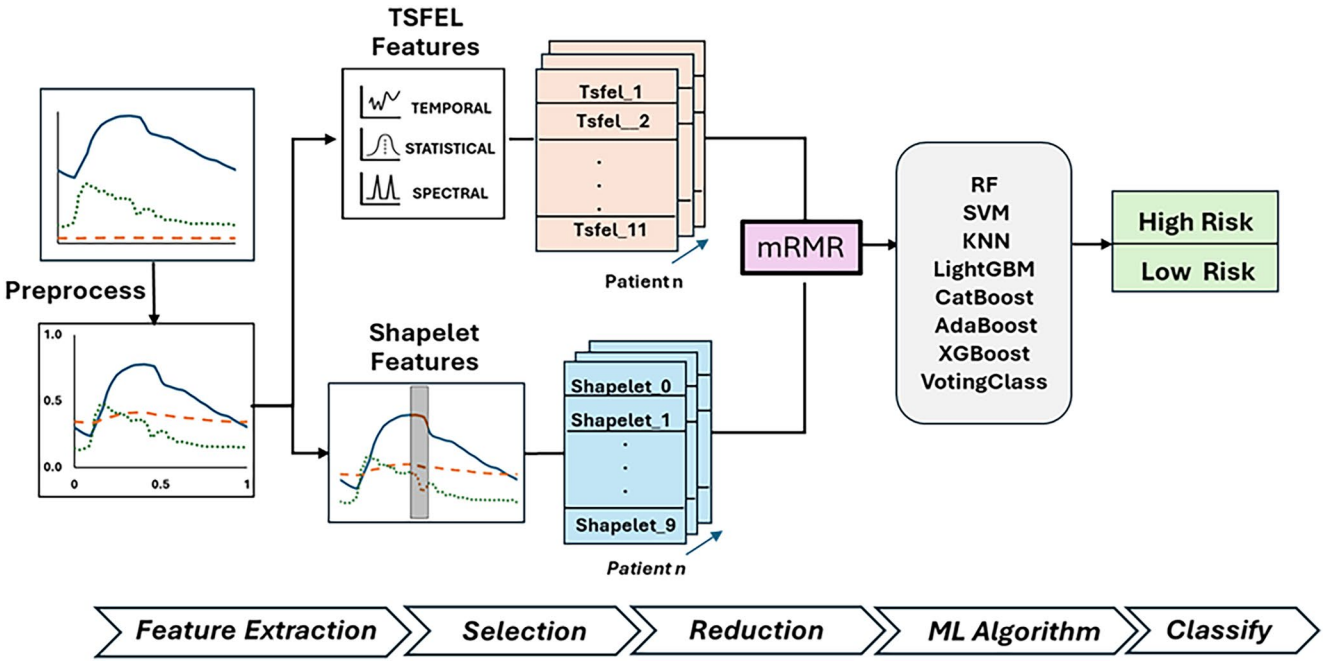

FIGURE 2 | Schematic pipeline for machine learning–based classification.

linear and nonlinear relationships while mitigating algorithm-specific biases. Distance-based modeling was performed using K-Nearest Neighbor (KNN), a non-parametric classifier that labels samples by majority vote among nearest neighbors [36]. Support Vector Machine (SVM) was applied for kernel-based modeling, constructing maximum-margin hyperplanes suitable for handling nonlinear boundaries in multidimensional feature spaces [37]. Tree-based modeling used Random Forest (RF), which provides robustness on tabular data, reduces variance, captures nonlinear interactions, and ranks feature importance [38]. Boosting methods included XGBoost, LightGBM, CatBoost, and AdaBoost, each offering unique advantages: XGBoost provides speed and regularization for high-dimensional data [39]; LightGBM enables fast, leaf-wise training [40]; CatBoost applies ordered boosting and handles categorical features effectively [41]; and AdaBoost iteratively reweights misclassified samples, though it can be sensitive to noise [42]. To enhance generalization and integrate complementary strengths, a Voting Classifier aggregated predictions from multiple models for final decisions.

Three synchronized waveforms—pressure, radial wall motion (diameter), and blood velocity—were acquired for each patient, with each waveform sampled at 128 time points over a single cardiac cycle. All time-series data were globally min–max normalized across subjects to ensure consistent inter-signal scaling and reduce bias during feature extraction and model training. The dataset was split into training (80%) and testing (20%) subsets using stratified sampling to preserve the original class distribution (1:3 high- to low-risk ratio). After splitting, hyperparameter optimization was performed for each traditional ML model using Grid Search with 5-fold cross-validation (GridSearchCV, scikit-learn [43]). The grid search systematically evaluated predefined parameter combinations to identify the configuration yielding the highest cross-validation accuracy. For each model type (e.g., tree-based, boosting, distance-based, and kernel-based), the optimal estimator was selected and subsequently applied to the testing set to assess generalization performance.

Model training and all algorithmic computations were performed using Google Colab for cloud-based experimentation and an NVIDIA GeForce RTX GPU for accelerated offline computation. All eight classifiers were trained using stratified 5-fold cross-validation to address the limited sample size and class imbalance. Performance was evaluated using test accuracy, area under the ROC curve (AUC), and F1-score, providing a comprehensive assessment of both overall classification accuracy and the balance between precision and recall. The workflow for data processing, feature extraction and selection, and ML classification is illustrated in Figure 2.

3 | Results

3.1 | Feature Selection

The initial feature set was reduced using the mRMR algorithm, decreasing signal-derived (TSFEL) features from 201 to 11 and shapelet features to 10. This dimensionality reduction was guided by cross-validation with RF models, which demonstrated improved classification performance using these subsets. The reduced TSFEL and shapelet features were then fused into a combined set, and mRMR was applied again to remove redundancy and enhance generalizability, yielding a final set of 15 features. This selection aligns with the commonly applied rule of maintaining approximately 10 samples per feature to avoid overfitting, given the dataset size of 150 samples. These 15 features were ultimately used as inputs for ML models.

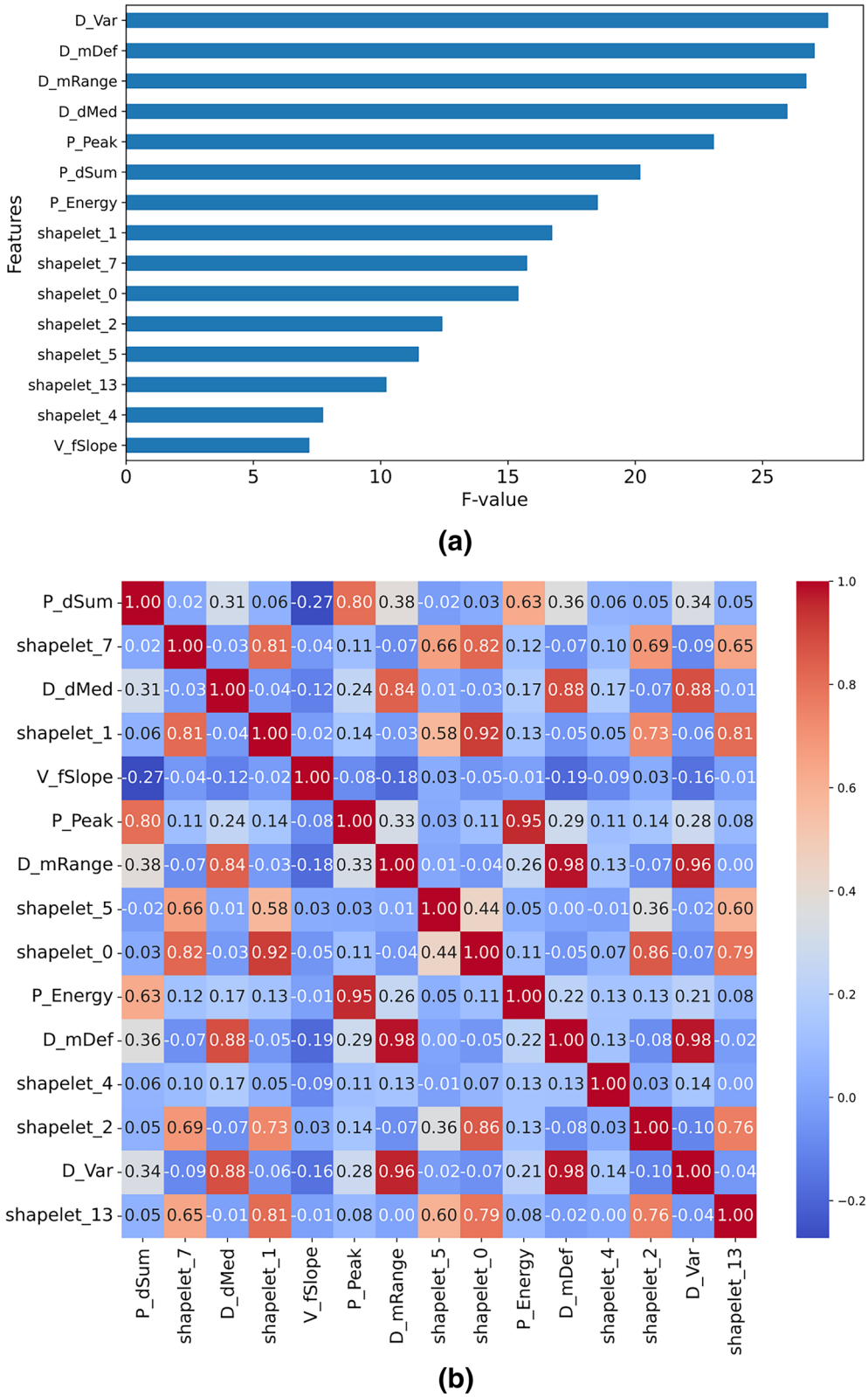

FIGURE 3 | (a) *F*-values and (b) correlation heatmap of the 15 selected features.

3.2 | Feature Characterization

The F-values (Figure 3a) and correlation heatmap (Figure 3b) for the 15 selected features are presented in Figure 3. Among the eight TSFEL features, four were extracted from the diameter waveform, three from the pressure waveform, and one from the velocity waveform. Seven additional features were selected from the Shapelet Transform. These shapelet features represent subsequences that capture both multivariate relationships across the diameter, pressure, and velocity waveforms, as well as

TABLE 1 | Description of eight features extracted using the TSFEL library.

Feature	Brief description	Physiological interpretation
D_mDef	The diameter signal's average absolute difference between each data point and the signal's mean	Measure of diameter variation during a cycle, which reflects arterial flexibility; smaller change indicates a stiffer or thickened arterial wall.
P_dSum	The pressure signal's total sum of absolute differences between consecutive data points	Measure of pressure time variation or gradient; higher values are commonly observed in hypertension and increased arterial stiffness.
P_Energy	The pressure signal's total contained energy, calculated as the sum of the squared absolute values	Measure of overall strength of the arterial pressure pulse; higher values are commonly associated with hypertension and increased arterial stiffness.
D_mRange	The diameter signal's range between the 75th and 25th percentiles	Measure of mean diameter during a cardiac cycle or the average vessel size; higher values indicate vascular remodeling.
D_Var	Quantifies the spread of data around the diameter signal's mean	Measure of diameter variation during a cycle; smaller variations indicate a stiffer or thickened arterial wall.
P_Peak	The highest value observed in the pressure signal	Measure of peak pressure or systolic pressure; higher values are indicative of hypertension and increased cardiovascular risk.
D_dMed	The diameter signal's median of absolute differences between consecutive data points	Measure of dimeter variation or gradient; higher values indicate a more compliant or thinner arterial wall, whereas lower values suggest arterial stiffening.
V_fSlope	The slope of spectral envelop of the velocity signal	Measures the concentration of velocity energy at low frequencies; higher values indicate a stiffer velocity waveform which is related to arterial compliance.

single-waveform patterns. A brief description of the eight signal derived (TSFEL) features and their physiological interpretations is provided in Table 1. Most features quantify the mean level, gradient, and amplitude of the diameter and pressure waveforms, as well as the spectral energy distribution of flow velocity. Collectively, these features reflect hemodynamic alterations associated with arterial stiffness, hypertension, and atherosclerotic vascular remodeling. Shapelet analysis identified phase-specific morphological features of the pressure, flow, and diameter waveforms with distinct physiological relevance. The temporal segments of the extracted shapelet examples are illustrated in Figure 4. Shapelets 1, 4, and 13 are associated with the systolic phase, whereas shapelet 2 reflects the early systolic phase. Shapelet 5 captures the region near peak systole and reflects peak pressure, flow, and maximal diameter expansion. In contrast, shapelets 0 and 7 represent diastolic waveform characteristics and primarily encode the relative magnitudes of pressure, flow, and diameter. Shapelet 7 is not shown in Figure 4 because its diastolic magnitude variations were minimal. Feature importance, quantified by MI scores for all 15 features, is shown in Figure 5. The top three features were associated with carotid diameter variation, pressure gradient, and energy. Among the shapelet features, shapelets 0, 1 and 2 exhibited the highest MI values. The selected 15 features were fused to a combined feature set, and eight ML models were applied to classify CVD risk.

3.3 | Classification Performance of ML Models

The performance metrics of the eight ML algorithms are summarized in Table 2. As shown in Table 2, RF exhibited the highest performance across all evaluated metrics, achieving an accuracy of 0.90, AUC of 0.95, and F1- score of 0.80. Among the remaining models, boosting and ensemble methods demonstrated comparatively strong performance, consistent with their ability to handle nonlinear feature interactions and reduce variance in small-sample settings. In contrast, SVM and KNN exhibited lower performance, likely due to their sensitivity to feature scaling, class overlap, and, in the case of KNN, the curse of dimensionality. To evaluate the effectiveness of combining signal-derived (TSFEL) and shapelet features, features were extracted separately from each method, and classification performance was compared using a RF classifier. To compare feature extraction strategies, 15 features were derived using signal-based TSFEL features, shapelet-based features, and their combination. The combined feature set achieved superior performance across all evaluation metrics (accuracy = 0.90, AUC = 0.95, F1-score = 0.80) compared with TSFEL-only features (accuracy = 0.77, AUC = 0.78, F1-score = 0.54) and shapelet-only features (accuracy = 0.80, AUC = 0.85, F1-score = 0.57). Based on these results, the combined 15-feature set was selected as the input for all subsequent analyses.

3.4 | Contribution of Multivariate Waveforms

Features were extracted from pressure, velocity, and diameter waveforms, as well as their interactions. To evaluate the contribution of each waveform, features were derived from individual and combined time-series data, and their classification performance was compared using a RF classifier (Table 3). Comparison of performance metrics across waveform

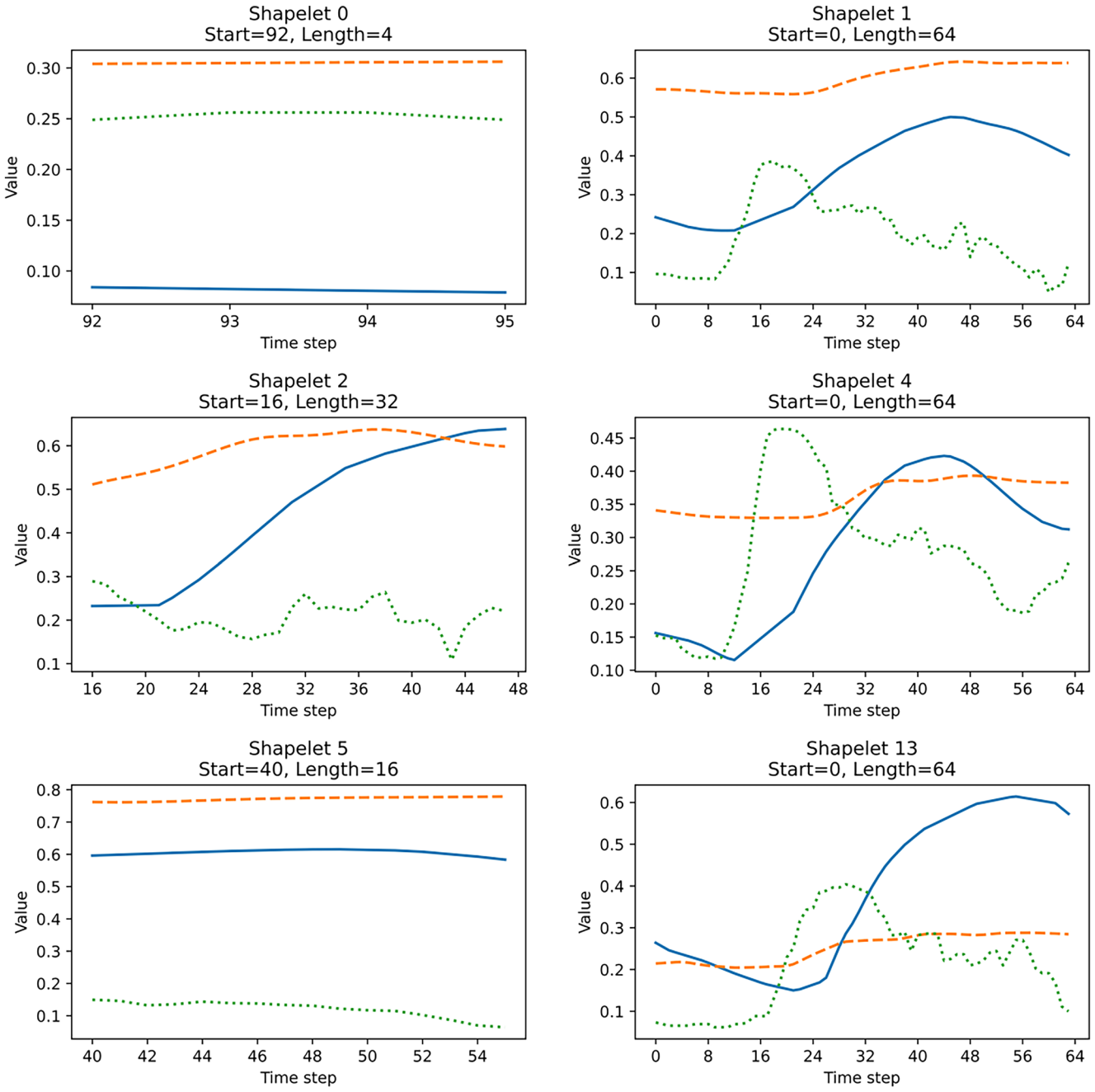

FIGURE 4 | Examples of selected shapelets. Solid, dashed, and dotted lines correspond to pressure, diameter, and velocity waveforms, respectively. The x-axis represents the temporal data point index, and the y-axis represents the normalized amplitude.

configurations demonstrated the advantage of integrating pressure, diameter, and velocity signals. Single-waveform models exhibit imbalanced performance profiles; in particular, the Pressure-only model achieves relatively high accuracy but a substantially lower AUC, indicating limited discriminative capability, especially for correctly identifying high-risk cases. Dual-waveform combinations partially improve metric balance but remain limited in either AUC or F1 score. ROC curves are shown in Figure 6. In contrast, the model combining all three waveforms consistently outperforms all other configurations across all metrics, demonstrating the most balanced and robust classification performance. These findings indicate that multivariate waveform analysis from carotid duplex sonography enables a more comprehensive characterization of atherosclerosis and improves ML-based CVD risk prediction.

4 | Discussion

Current clinical assessments based on carotid duplex sonography primarily focus on static plaque morphology and peak flow velocity, despite the modality's ability to provide rich, time-resolved information on arterial dynamics. In this study, we instead utilize the full temporal waveforms extracted from Doppler ultrasound to capture physiologically meaningful interactions between blood flow and arterial wall mechanics. The synchronized pressure, diameter, and velocity waveforms—and

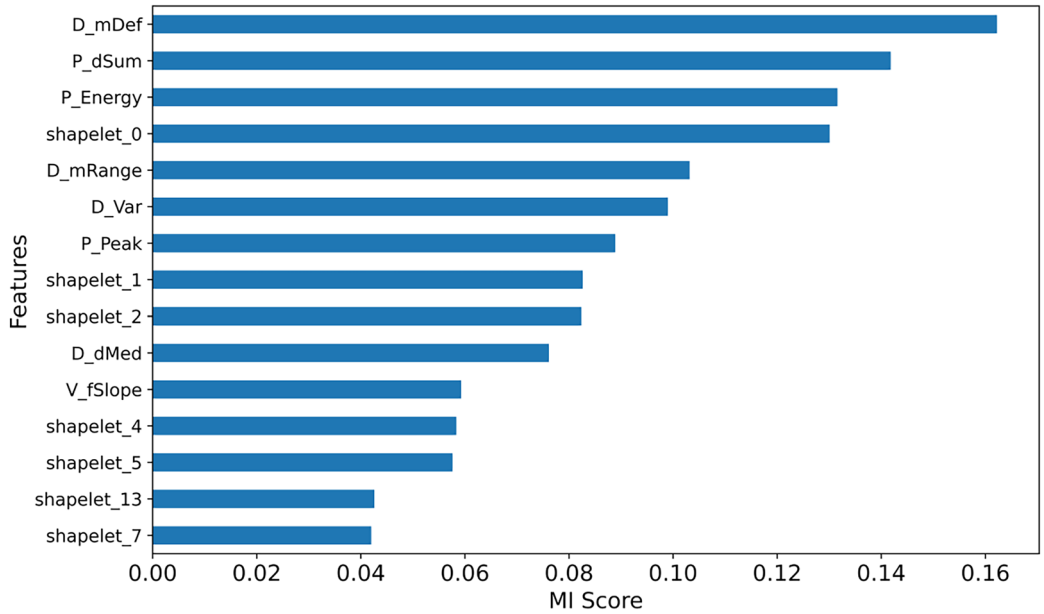

FIGURE 5 | Mutual information (MI) scores of the 15 features, indicating their relative importance for classification.

TABLE 2 | Classification performance metrics of the eight evaluated ML models.

Models	Accuracy	AUC	F1-score
Random forest	0.90	0.95	0.80
XGBoost	0.83	0.76	0.75
LightGBM	0.87	0.80	0.79
CatBoost	0.80	0.80	0.64
AdaBoost	0.86	0.82	0.79
Support vector machine	0.66	0.61	0.54
K-nearest neighbor	0.80	0.61	0.57
Voting classifier	0.80	0.62	0.64

TABLE 3 | Performance of RF classifiers using different combinations of input waveforms.

Waveforms	Accuracy	AUC	F1-score
Pressure	0.77	0.67	0.61
Diameter	0.83	0.87	0.79
Velocity	0.77	0.57	0.54
Pressure + diameter	0.73	0.78	0.58
Diameter + velocity	0.73	0.74	0.63
Velocity + pressure	0.70	0.71	0.50
Pressure + diameter + velocity	0.90	0.95	0.80

their temporal interrelationships—encode information related to plaque mechanical properties, luminal narrowing, and arterial stiffening. For example, the pressure–diameter relationship reflects arterial wall viscoelasticity, which changes with plaque progression, including fibrosis, lipid accumulation, smooth muscle cell proliferation, and calcification [44]. Likewise, the coupling between pressure and flow waveforms characterizes arterial impedance, influenced by distal stenosis, luminal narrowing, and vascular stiffening [45, 46]. Although viscoelasticity and impedance are established biomarkers of vascular health and CVD risk, their reliable estimation from in vivo dynamic signals is challenging due to the complex and incompletely defined interactions among pressure, diameter, and velocity waveforms. This complexity limits the effectiveness of traditional analytical or model-based approaches. To overcome these constraints, we implemented a ML framework that directly identifies discriminative patterns from multivariate Doppler-derived waveforms without relying on explicit biomechanical modeling. The findings indicate that carotid ultrasound–derived dynamic waveforms provide physiologically informative inputs for CVD risk classification and underscore the largely underexplored diagnostic potential of Doppler ultrasound beyond conventional scalar indices. This framework offers a practical and scalable pathway for translating computational biomechanics into clinically applicable ultrasound-based risk stratification.

This study further demonstrates that multivariate time-series analysis of carotid arterial waveforms can effectively support CVD risk classification. The proposed framework achieved the most balanced and robust performance when integrating pressure, diameter, and velocity signals, outperforming single- and dual-waveform configurations across all evaluation metrics. In contrast, single-waveform models exhibited imbalanced performance—for example, the pressure-only model showed relatively high accuracy but a substantially lower AUC, indicating limited discriminative capability for high-risk cases. This finding highlights the importance of capturing complementary physiological information across multiple waveform modalities. Specifically, pressure waveforms primarily reflect hemodynamic load, diameter waveforms encode arterial compliance and wall mechanics, and velocity waveforms represent flow dynamics and disturbance associated with stenosis. The

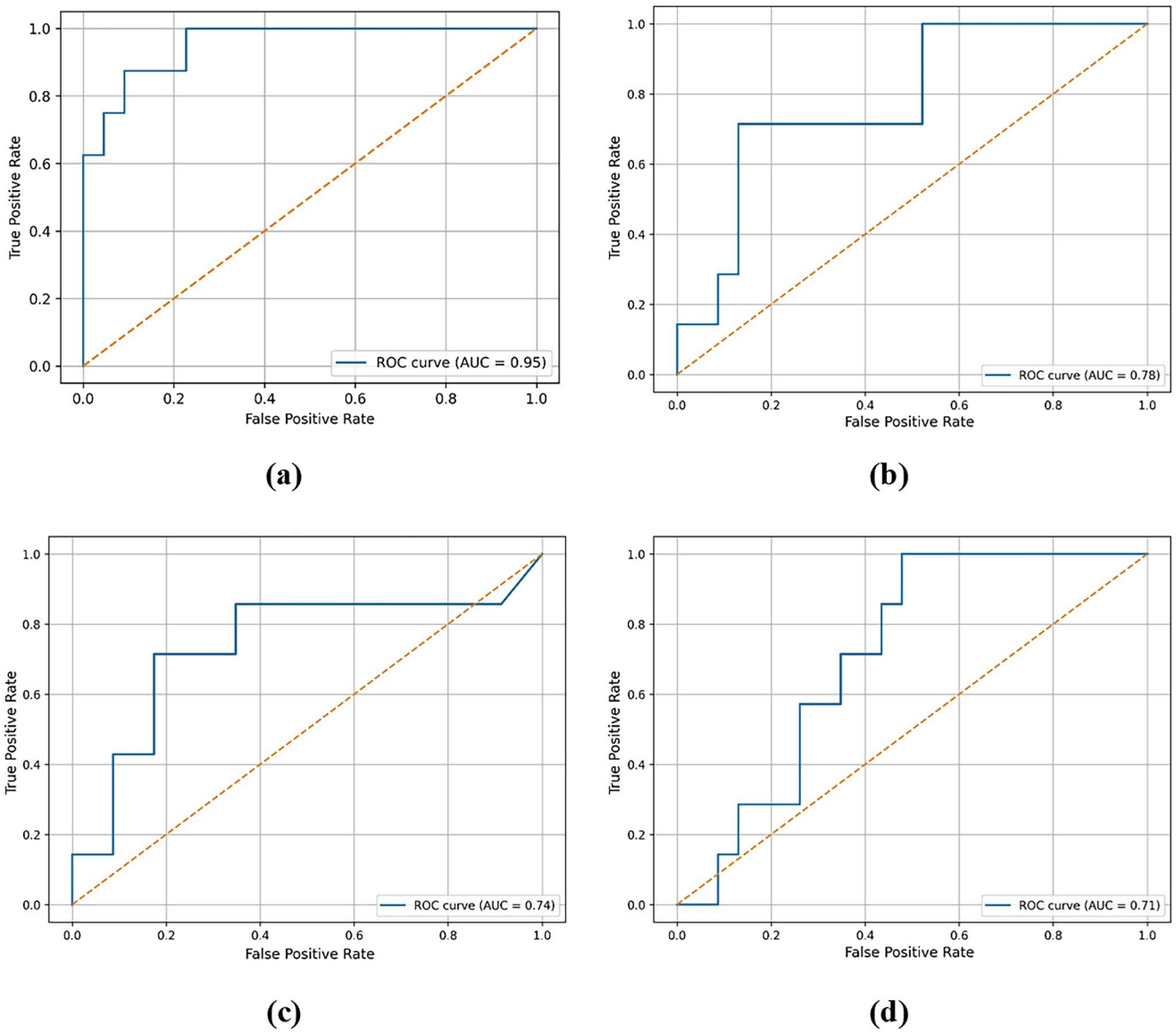

FIGURE 6 | ROC curves for the RF classifiers using different combinations of input waveforms: (a) pressure + diameter + velocity; (b) pressure + diameter; (c) diameter + velocity; (d) velocity + pressure.

superior performance of the combined model suggests that the interaction among these signals provides a more comprehensive representation of vascular function and pathology.

Importantly, the selected 15 features exhibit clear physiological relevance and are consistent with established biomarkers of cardiovascular risk. Signal-based features derived from pressure and diameter waveforms, such as amplitude, mean level, and temporal gradients, are closely associated with arterial stiffness, compliance, and hemodynamic load. For example, increased pulse pressure amplitude and steeper systolic upstroke have been linked to reduced arterial compliance and increased vascular stiffness, both of which are well-established predictors of cardiovascular events [15]. Similarly, variations in diameter waveforms reflect arterial distensibility and wall elasticity, which decrease with aging and atherosclerotic progression. Features derived from velocity waveforms, including spectral energy distribution, are related to flow dynamics and disturbed hemodynamics, which have been associated with stenosis severity and endothelial dysfunction [10]. In addition, the shapelet-based features capture localized, phase-specific waveform patterns that reflect underlying vascular physiology. For instance, shapelets corresponding to the systolic phase may encode rapid pressure and flow acceleration, influenced by ventricular ejection and proximal arterial stiffness, whereas diastolic shapelets reflect peripheral resistance and wave reflection phenomena [12]. These temporal patterns are known to be altered in the presence of arterial stiffening and atherosclerosis, where increased wave reflection and impedance mismatch lead to characteristic changes in waveform morphology [47]. Collectively, these findings indicate that the extracted features are not merely data-driven constructs but are physiologically grounded representations of vascular function and pathology, supporting their relevance for CVD risk assessment. While the extracted features are statistical in nature, this choice was motivated by the challenges associated with directly estimating physiological parameters (e.g., arterial stiffness or impedance) from in vivo signals, which typically require strong modeling

assumptions and precise calibration. In contrast, statistical features provide a more robust and model-agnostic representation of waveform characteristics while still preserving meaningful physiological information.

Despite these promising findings, several limitations should be acknowledged. First, the relatively small dataset size necessitated the use of feature-based machine learning models, which, while interpretable, may not capture highly complex nonlinear relationships compared to deep learning approaches. Second, TPA-based labeling is subject to operator dependence, two-dimensional imaging constraints, and potential variability in threshold selection, which may limit generalizability. Although TPA is a well-established marker of atherosclerotic burden, it was derived from two-dimensional ultrasound images requiring manual or semi-manual plaque delineation, making it sensitive to operator dependency, probe positioning, and slice selection. Prior studies report variability depending on plaque size and methodology (coefficient of variation (CV) ~2% to > 25% for 3D, 5%–8% for 2D measurements) [48, 49], even though high Intraclass Correlation Coefficients (ICCs) can be achieved under controlled conditions [50]. In contrast, waveform-derived features are extracted from temporally continuous signals using semi-automated tracking, reducing reliance on single-frame annotation and benefiting from temporal redundancy. In our dataset, diameter measurements showed relatively low variability (CV ≈5%), suggesting improved measurement stability. While a direct sensitivity analysis for TPA was not feasible due to the lack of repeated annotations, these observations suggest that waveform-based features may provide a more robust and complementary representation of vascular dynamics. Third, temporal synchronization of multimodal signals was performed retrospectively using ECG gating rather than simultaneous acquisition, which may introduce phase mismatches due to heart rate variability or detection errors. Additionally, the use of a single representative cardiac cycle per subject limits the assessment of intra-subject variability. Finally, the multimodal acquisition process may pose challenges for scalability and automation in clinical practice. Future studies with larger, multicenter cohorts, fully synchronized multi-cycle acquisitions, and prospective outcome validation are needed to confirm robustness and establish the clinical utility of this approach.

5 | Conclusion

This study demonstrates that ML can effectively classify CVD risk using carotid time-series data, including radial wall motion and flow velocity, which are dynamic metrics not routinely evaluated in clinical practice. By combining signal-derived and shapelet-based features for multivariate time series dataset, RF classifiers achieved high performance (accuracy: 0.90, AUC: 0.95, F1-score: 0.80). These results underscore the potential of ultrasound-based time-series analysis as a complementary, data-driven approach to conventional static imaging for CVD risk assessment.

Author Contributions

Belilla Yonas Befirdu: data curation, formal analysis, methodology, validation, visualization, writing-original draft; **Duc-Manh Dinh:** data curation, methodology, visualization; **Eui-Young Choi:** conceptualization, supervision, validation; **Kyehan Rhee:** conceptualization, funding acquisition, project administration, supervision, writing-review and editing.

Funding

Research supported by the National Research Foundation of Korea (NRF) grant funded by the Korea government (MSIT) (grant no. 2023R1A2C1003364).

Ethics Statement

This study was performed in line with the principles of the Declaration of Helsinki. Approval was granted by the Institutional Review Board of Gangnam Severance Hospital (IRB No. 3-2020-01420). The requirement for informed consent was waived because this retrospective study involved only the analysis of previously acquired anonymized medical images.

Conflicts of Interest

The authors declare no conflicts of interest.

Data Availability Statement

The data that support the findings of this study are openly available in Github at https://github.com/YonasBefirdu/ML-Based-CVD-Risk-Classification.

References

1. S. S. Ho, "Current Status of Carotid Ultrasound in Atherosclerosis," *Quantitative Imaging in Medicine and Surgery* 10, no. 3 (2020): 515–523.

2. M. Alexandratou, A. Papachristodoulou, X. Li, et al., "Advances in Noninvasive Carotid Wall Imaging With Ultrasound: A Narrative Review," *Journal of Clinical Medicine* 11, no. 20 (2022): 6196.

3. S. Bir and R. Kelley, "Carotid Atherosclerotic Disease: A Systematic Review of Pathogenesis and Management," *Brain Circulation* 8, no. 3 (2022): 127–136.

4. A. M. Johri, V. Nambi, T. Z. Naqvi, et al., "Recommendations for the Assessment of Carotid Arterial Plaque by Ultrasound for the Characterization of Atherosclerosis and Evaluation of Cardiovascular Risk," *Journal of the American Society of Echocardiography* 33, no. 8 (2020): 917–933.

5. L. E. Chambless, G. Heiss, A. R. Folsom, et al., "Association of Coronary Heart Disease Incidence With Carotid Arterial Wall Thickness and Major Risk Factors: The ARIC Study, 1987–1993," *American Journal of Epidemiology* 146, no. 6 (1997): 483–494.

6. M. L. Bots, A. W. Hoes, P. J. Koudstaal, A. Hofman, and D. E. Grobbee, "Common Carotid Intima-Media Thickness and Risk of Stroke and Myocardial Infarction: The Rotterdam Study," *Circulation* 96, no. 5 (1997): 1432–1437.

7. J. D. Spence, M. Eliasziw, M. DiCicco, D. G. Hackam, R. Galil, and T. Lohmann, "Carotid Plaque Area: A Tool for Targeting and Evaluating Vascular Preventive Therapy," *Stroke* 33, no. 12 (2002): 2916–2922.

8. M. L. Grønholdt, "Ultrasound and Lipoproteins as Predictors of Lipid-Rich, Rupture-Prone Carotid Plaque," *Arteriosclerosis, Thrombosis, and Vascular Biology* 19, no. 1 (1999): 2–13.

9. A. Oglat, M. Z. Matjafri, N. Suardi, M. A. Oqlat, M. A. Abdelrahman, and A. A. Oqlat, "A Review of Medical Doppler Ultrasonography of Blood Flow in General and Especially in Common Carotid Artery," *Journal of Medical Ultrasound* 26, no. 1 (2018): 3–13.

10. A. N. Nicolaides, S. K. Kakkos, M. Griffin, et al., "Severity of Asymptomatic Carotid Stenosis and Risk of Ipsilateral Hemispheric Ischaemic Events: Results From the ACSRS Study," *European Journal of Vascular and Endovascular Surgery* 30, no. 3 (2005): 275–284.

11. R. G. Gosling and D. H. King, "Arterial Assessment by Doppler-Shift Ultrasound," *Proceedings of the Royal Society of Medicine* 67, no. 6 (1974): 447–449.

12. W. W. Nichols, M. O'Rourke, and C. Vlachopoulos, *Mcdonald's Blood Flow in Arteries*, 6th ed. (CRC Press, 2011).

13. K. V. Ramnarine, T. C. Hartshorne, Y. Sensier, et al., "Tissue Doppler Imaging of Carotid Plaque Wall Motion: A Pilot Study," *Cardiovascular Ultrasound* 1 (2003): 17.

14. J. Alastruey, P. Charlton, V. Bikia, et al., "Arterial Pulse Wave Modeling and Analysis," *American Journal of Physiology. Heart and Circulatory Physiology* 325, no. 1 (2023): H1–H29.

15. C. Vlachopoulos, K. Aznaouridis, and C. Stefanadis, "Prediction of Cardiovascular Events With Arterial Stiffness," *Journal of the American College of Cardiology* 55, no. 13 (2010): 1318–1327.

16. D. Dinh, B. Y. Befirdu, and K. Rhee, "Enhancing Cardiovascular Risk Prediction," *Computer Methods in Biomechanics and Biomedical Engineering. Computer Methods in Biomechanics and Biomedical Engineering* (2025): 1–12, https://doi.org/10.1080/10255842.2025.2475479.

17. B. Hametner, T. Weber, C. Mayer, J. Kropf, and S. Wassertheurer, "Calculation of Arterial Characteristic Impedance," *Mathematical and Computer Modelling of Dynamical Systems* 19, no. 4 (2013): 319–330.

18. J. Shin, E. Choi, H. Kwon, and K. Rhee, "Estimation of Viscoelasticity of a Carotid Artery," *Medical Engineering & Physics* 108 (2022): 103886.

19. X. Zhang, D. Wu, H. Li, Y. Fang, H. Xiong, and Y. Li, "Early Diagnosis of Carotid Artery Stenosis," *Bioengineering* 9, no. 9 (2022): 422.

20. X. Huang, Y. Zhang, M. Qian, et al., "Classification of Carotid Plaque Echogenicity," *Journal of Ultrasound in Medicine* 35, no. 10 (2016): 2253–2261.

21. L. Zhang, Q. Lyu, Y. Ding, C. Hu, and P. Hui, "Texture Analysis Based on Vascular Ultrasound to Identify Vulnerable Carotid Plaques," *Frontiers in Neuroscience* 16 (2022): 885209.

22. A. Tamborini, A. Aghilinejad, R. V. Matthews, and M. Gharib, "Machine Learning Reconstruction of Left Ventricular Pressure From Peripheral Waveforms. JACC," *Advances* 4, no. 9 (2025): 102104.

23. G. F. Mitchell, J. Rong, M. G. Larson, et al., "Vascular Age Assessed From an Uncalibrated, Noninvasive Pressure Waveform by Using a Deep Learning Approach: The AI-vascularAge Model," *Hypertension* 81, no. 1 (2024): 193–201.

24. B. Ambale-Venkatesh, X. Yang, C. O. Wu, et al., "Cardiovascular Event Prediction by Machine Learning: The Multi-Ethnic Study of Atherosclerosis," *Circulation Research* 121, no. 9 (2017): 1092–1101.

25. A. Fazio, R. Bella, A. Basile, and V. Cantisani, "Imaging of Carotid Stenosis: Where Are we Standing? Comparison of Multiparametric Ultrasound, CT Angiography, and MRI Angiography, With Recent Developments," *Diagnostics (Basel, Switzerland)* 14, no. 16 (2024): 1708.

26. G. Zahnd, M. Orkisz, E. E. Serrano, and D. Vray, "CAROLAB: A Platform to Analyze Carotid Ultrasound Data," in *IEEE International Ultrasonics Symposium (IUS)* (Institute of Electrical and Electronics Engineers (IEEE), 2019).

27. H. Mohammadi, B. Tarvirdizadeh, K. Alipour, and M. Ghamari, "Cuff-Less Blood Pressure Monitoring via PPG Signals Using a Hybrid CNN-BiLSTM Deep Learning Model With Attention Mechanism," *Scientific Reports* 15 (2025): 22229.

28. E. Gudmundsson, G. Björnsdottir, S. Sigurdsson, et al., "Carotid Plaque Is Strongly Associated With Coronary Artery Calcium and Predicts Incident Coronary Heart Disease in a Population-Based Cohort," *Atherosclerosis* 346 (2022): 117–123.

29. A. Adams, W. Bojara, and M. Romanens, "The Determination of Plaque Burden on the Carotid Artery Improves Risk Prediction," *Cardiology Research* 11, no. 4 (2020): 233–238.

30. E. Mathiesen, S. Johnsen, T. Wilsgaard, K. Bønaa, M. Løchen, and I. Njølstad, "Carotid Plaque Area and Intima-Media Thickness in Prediction of First-Ever Ischemic Stroke," *Stroke* 42, no. 4 (2011): 972–978.

31. H. S. Kim and K. I. Cho, "Association of Carotid Artery Parameters of Atherosclerosis in Coronary Artery Disease," *Journal of Cardiovascular Ultrasound* 21, no. 2 (2013): 72–80.

32. M. Barandas, D. Folgado, L. Fernandes, et al., "TSFEL: Time Series Feature Extraction Library," *SoftwareX* 11 (2020): 100456.

33. C. Ding and H. Peng, "Minimum Redundancy Feature Selection From Microarray Gene Expression Data," *Journal of Bioinformatics and Computational Biology* 3, no. 2 (2005): 185–205.

34. A. Boström and A. Bagnall, "A Shapelet Transform for Multivariate Time Series Classification," *arXiv* (2017) preprint arXiv:1711.11343.

35. S. Garcia, J. Luengo, J. Sáez, V. López, and F. Herrera, "A Survey of Discretization Techniques," *IEEE Transactions on Knowledge and Data Engineering* 25, no. 4 (2012): 734–750.

36. T. Cover and P. Hart, "Nearest Neighbor Pattern Classification," *IEEE Transactions on Information Theory* 13, no. 1 (1967): 21–27.

37. C. Cortes and V. Vapnik, "Support-Vector Networks," *Machine Learning* 20, no. 3 (1995): 273–297.

38. L. Breiman, "Random Forests," *Machine Learning* 45, no. 1 (2001): 5–32.

39. T. Chen and C. Guestrin, "XGBoost: A Scalable Tree Boosting System," in *Proceedings of the 22nd ACM SIGKDD International Conference on Knowledge Discovery and Data Mining* (Cornell University (arXiv), 2016).

40. G. Ke, Q. Meng, T. Finley, et al., "LightGBM: A Highly Efficient Gradient Boosting Decision Tree," in *Advances in Neural Information Processing Systems* (Cornell University (arXiv), 2017).

41. L. Prokhorenkova, G. Gusev, A. Vorobev, A. V. Dorogush, and A. Gulin, "CatBoost: Unbiased Boosting With Categorical Features," in *Advances in Neural Information Processing Systems* (Cornell University (arXiv), 2018).

42. Y. Freund, R. E. Schapire, and N. Abe, "A Short Introduction to Boosting," *Journal of the Japanese Society for Artificial Intelligence* 14 (1999): 771–780.

43. F. Pedregosa, G. Varoquaux, A. Gramfort, et al., "Scikit-Learn: Machine Learning in Python," *Journal of Machine Learning Research* 12 (2011): 2825–2830.

44. D. Bia, Y. Zócalo, E. Cabrera-Fischer, S. Wray, and R. Armentano, "Quantitative Analysis of the Relationship Between Blood Vessel Wall Constituents and Viscoelastic Properties," *Scientific World Journal* 2014 (2014): 142421.

45. D. Fitchett and M. F. O'Rourke, "Pulsatile Haemodynamics and Arterial Impedance," in *Cardiopulmonary Monitoring*, ed. S. Magder, A. Malhotra, K. A. Hibbert, and C. C. Hardin (Springer, 2021), https://doi.org/10.1007/978-3-030-73387-2_9.

46. S. Niroumandi, R. Alavi, A. Wolfson, A. Vaidya, and N. Pahlevan, "Assessment of Aortic Characteristic Impedance and Arterial Compliance From Non-Invasive Carotid Pressure Waveform," *American Journal of Cardiology* 204 (2023): 195–199.

47. A. Avolio, B. E. Westerhof, M. Siebes, and J. V. Tyberg, "Arterial Hemodynamics and Wave Analysis in the Frequency and Time Domains," *Medical & Biological Engineering & Computing* 47, no. 2 (2009): 107–110.

48. A. Landry, J. D. Spence, and A. Fenster, "Measurement of Carotid Plaque Volume by 3-Dimensional Ultrasound," *Stroke* 35, no. 4 (2004): 864–869.

49. I. Stenudd, E. Sjödin, E. Nyman, P. Wester, E. Johansson, and C. Grönlund, "Ultrasound Risk Marker Variability in Symptomatic Carotid Plaque: Impact on Risk Reclassification and Association With Temporal Variation Pattern," *International Journal of Cardiovascular Imaging* 36, no. 6 (2020): 1061–1068.

50. M. Ludwig, T. Zielinski, D. Schremmer, and K. O. Stumpe, "Reproducibility of 3-Dimensional Ultrasound Readings of Volume of Carotid Atherosclerotic Plaque," *Cardiovascular Ultrasound* 26, no. 6 (2008): 42.